MICROSTRUCTURE, MINERALOGY AND PHYSICAL PROPERTIES OF GROUND FLY ASH BASED GEOPOLYMERS

FERENC MÁDAI*, #FERENC KRISTÁLY*, GÁBOR MUCSI**

*University of Miskolc, Institute of Mineralogy and Geology,
Miskolc-Egyetemváros, Hungary
**University of Miskolc, Institute of Raw Materials Preparation and Environmental Processing,
Miskolc-Egyetemváros, Hungary

#E-mail: kristalyf@gmail.com

This paper is focused on the utilization of deposited fly ash as a main component of geopolymer. After determination of particle size distribution, moisture content, real and bulk density and specific surface area of the raw fly ash, mechanical activation was performed by laboratory scale ball mill. This step is introduced for improving the reactivity of raw material. Then test specimens were produced by geopoliomerisation using a caustic spent liquor (NaOH). Compressive strength was determined on cilindrical specimens. Finally, samples of the ground fly ash based geopolymer specimens were analyzed by X-ray diffraction, optical and scanning electron microscopy. Results prove that geopolymer production with proper strength from the investigated F-type deposited fly ash is possible. The uniaxial compressive strength of obtained composites strongly depends on the fineness of the ground fly ash.
XRD results show that comparing the crystalline components for different geopolymer samples, zeolite-A appears and its amount increases gradually from 0T sample till 30T and then decreases for 60T sample. The same trend holds for sodalite type structure phases, however its amount is much lower than for zeolite-A.
SEM+EDS investigation revealed that Na-content is elevated in the interstitial fine-grained matrix, especially for the 30T sample when highest strength was observed. Si and Al are abundant mainly in anhedral and spherical grains and in rarely occurring grains resembling some crystal shape.

INTRODUCTION

Geopolymers or also known as inorganic polymers or "artificial stones" are alumino-silicate materials, which exhibit improved physical and chemical properties. These materials are prepared in alkali-hydroxide solution media (NaOH, KOH), through the binding of silicate groups by alkaline cations. The result is a solid, strengthened (hydrated) matrix, mainly in amorphous state, but also containing newly crystallized phases. It is important to note that the activation reaction rate depends on several factors such as the particle size and the mineralogical composition of the starting material, its vitreous phase content as well as the type and concentration of the activator [1]. For a better polymerization NaOH solution is preffered [2] and soluble Na- or K-silicates in the media catalyzes the process [3]. Due to their special characteristics – high durability, acid- and fire resistance, low shrinkage, etc. [4] - geopolymers can be applied in diverse range, e.g. non-structural elements, concrete pavements and products, containment and immobilization of toxic or hazardous and radioactive wastes, advanced structural tooling, refractory ceramics and fire resistant composites used in buildings. The main advantage of geopolymer production is the drastic reduction of CO_2 generation during the process.

According to [5], the empirical formula of geopolymers, if taken as poly-sialates, may be given in the form:

$$M_n\{-(Si–O_2)_z–Al–O\}_n \cdot wH_2O \qquad (1)$$
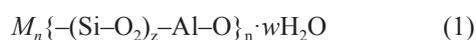
where M is a cation such as K^+, Na^+ or Ca^{2+}; the symbol "–" means the presence of a bond, n is the degree of polymerization, w is the number of associated water molecules and z is 1, 2 or 3. Other cations such as Li^+, Ba^{2+}, NH^{4+} and H_3O^+ may also be present [6]. Starting materials for the process are preferably low grain sized, high amorphous (glass) containing silicate materials, such as fly ash, volcanic tuff or metakaolin.

Power station fly ash is the by-product of the coal firing energy production which is generated in huge amounts worldwide – only in China and India about 300 million tons per year, in Europe this number is over one hundred million tons [7, 8, 9]. Depositing this enormous quantity is problematic from several points of view. Fly ash dumpsites reduce the valuable lands

from agricultural activity and creates environmental risk and pollution. This makes it important to develop new technologies allowing to recycle the fly ash into value-added products. The utilization of this by-product as a geopolymer raw material contributes to solve this problem. Additionally, fly ash based geopolymers have good mechanical properties and immobilization capacity of toxic elements and materials.

Several papers [1, 10, 11] deal with the investigation of fly ash as a geopolymer raw material. However these experiments apply only "fresh" (dry) fly ash (originated from the power station directly) as starting material, not a long-term deposited one. There are also several recent papers regarding mechanically activated fly ash or slag based geopolymers. Investigations carried out by [12] used mainly high energy density mills, such as vibratory and stirred media mill. It was revealed that besides the particle size distribution or the specific surface area the reactivity depended on the mill type used for the mechanical activation of the raw material. The effect of mechanical activation of raw material on geopolymers was investigated also by [13, 1, 14, 15].

Somna et al. [16] studied geopolymers obtained from similar raw materials, with similar processing. Ground fly ash with a median particle size of 10.5 μm was used as raw material mixed with NaOH as an alkali activator. Results indicated that ground fly ash gave higher strength geopolymer matrix as compared to unground material. The compressive strengths at 28 days of 20.0 - 23.0 MPa were obtained. Diaz et al. [17] investigated the suitability of fly ash stock piles for geopolymer manufacturing focusing on the chemical analyses, X-ray diffraction (XRD) and particle size distribution (PSD) of five fly ashes from coal-fired power plants. It was established that fly ash characteristics such as particle size distribution, amorphous material content and type (from XRD) play an important role in the fresh and hardened properties of the resulting geopolymer. Van Riessen & Chen-Tan [18] studied the beneficiation of fly ash in a three stage procedure using sieving, milling and magnetic separation to improve fly ash homogeneity and reactivity. It was stated that the proportion of amorphous content increased at each stage of beneficiation, resulting in increased reactivity, additionally different geopolymer properties, extend the range of applications for which geopolymers can be used.

Paul et al. [19] carried out high energy ball milling of class F fly ash in order to convert it into nanostructured material. They found that the surface of the produced nanometer size fly ash has become more active as observed by FTIR studies. Morphological studies revealed that the surface of the nanostructured fly ash is more uneven and rough with irregular shape, as compared to fresh fly ash which are mostly spherical in shape. Fu et al. [20] investigated the physical-chemical characteristics of mechanically-treated circulating fluidized bed combustion fly ash. It was found that the water requirement decreases with prolonged grinding time, and slightly increases during the last stage of grinding. The pH of ground fly ash is greater than that of the original fly ash, indicating that ground samples react more rapidly with water. The amount of crystalline components decreased by grinding, while the FWHM of peaks for residual crystalline phases increased. This allows amorphization and crystallite reduction to nano-meter scale, resulting in higher reactivity than the original fly ash.

Hounsi et al. [14] investigated the influence of mechanical activation of raw kaolin on the final compressive strength of geopolymers. Mechanical activation was performed by dry ball-milling for 1 hour. Results showed that without mechanical activation, the optimal curing condition was 24 h at 70°C and the compressive strength was 15 MPa after 28 days of ageing. After mechanical activation, improvement of the compressive strength was obtained with a curing time of 72 h at 70°C (35 % increase) or with a curing temperature of 100°C (76 % improvement). The formation of alkaline aluminosilicate glass and new crystalline hydrated phases controlled the strength development of geopolymers while the occurrence of carbonated species was responsible for the degradation of mechanical properties.

One aim of this paper is to investigate the changes in composition – chemical and mineralogical, microstructure, and physical properties of fly ash based geopolymer samples. Another goal was to examine the effect of mechanical activation (by grinding) on geopolymer product, using a decades ago deposited F-type fly ash as starting material. In this paper the results of these experiments are presented. A crucial task was to determine the degree of crystallinity and its change during polymerization, since it is considered one of the most important properties of geopolymers and their raw materials [21] as function of grinding fineness.

EXPERIMENTAL

The main raw material of our experimental investigation is deposited Class F (ASTM classification) coal-fired power station fly ash from Tiszaújváros (Hungary) dumpsite. The chemical composition of fly ash is presented in Table 1. From this analysis the SiO_2/Al_2O_3 ratio was found to be 2.26, combined SiO_2, Al_2O_3 and Fe_2O_3 content of the fly ash was 90.61 %. The dried raw fly ash was ground in a batch ball mill with steel grinding media for 10, 20, 30 and 60 minutes. Than the spent liquor alkaline activator with 190 g·l^{-1} Na$_2$O concentration was added in a proper quantity (L/S = 1/2) to the fly ash and they were mixed carefully. In our case caustic spent liquor from MAL PLC. (bauxite refinery company) was used as activator. The geopolymer paste obtained was poured into a cylindrical mould with a size of Ø 50 × 50 mm, compacted by vibration and kept in

95 % relative humidity for 3 hours. Then the specimens were released from the mould and then dried at ambient temperature for 16 hours followed by heat treatment at 150°C in an electrical furnace for 4 hours and then cooled to room temperature for further tests. To study the compositional and microstructural properties, samples from the original, untreated, raw and ground fly ash as well as the geopolymer materials were investigated. The samples are referred later in the text according to the sample codes given in Table 2. Particle size distribution for fly ash was measured with Horiba 950 LA laser analyzer analyzer in wet mode using distilled water as dispersing media and sodium-pyro-phosphate as dispersing agent applying the Mie-theory as evaluation method. The "outer" specific surface area (SSA) was calculated by the Horiba PSA from the particle size distribution data using the power function method. Additionally, the total SSA was measured by BET method using MICROMERITICS TRISTAR 3000 apparatus. Real and bulk density (pycnometer method) and the moisture content were also determined (averaged values of two parallel measurements, Table 3).

Table 1. Chemical composition of the deposited Class F fly ash (Tiszaújváros) (ED-XRF measurments, Cemkut Ltd.).

Component	Weight percents
SiO_2	59.05
Fe_2O_3	5.42
Al_2O_3	26.14
CaO	2.30
MgO	1.12
SO_3	0.25
L.O.I.	2.85

Table 2. Sample codes used for the different analysed samples.

Sample types	Unground	Grinding time (minutes)			
		10	20	30	60
untreated fly ash	0U	–	–	–	–
fly ash after geopolymerisation	0T	10T	20T	30T	60T

Table 3. Main physical parameters of the raw materials.

Material property	Raw fly ash
Particle density (kg·dm^{-3})	1.74
Bulk density (kg·dm^{-3})	0.71
Moisture content (%)	7.68
Specific surface area (cm^2·g^{-1})	501.37
Median of particle size distribution (μm)	119.72

The composition of samples was investigated by X-ray powder diffraction (XRPD, Bruker D8 Advance diffractometer, Cu-K$_\alpha$,40 kV and 40 mA in parallel-beam geometry by Göbel-mirror). Thin sections and polished block specimens were prepared from samples 0T, 10T, 20T, 30T and 60T. Untreated samples were investigated only as powder specimens. Optical microscopy in transmitted plane polarized light (OMPL) and scanning electron microscopy (SEM, JEOL 8600 Superprobe, 15 kV and 20 nA) was used for texture analysis. Energy dispersive spectrometry (EDS, standardless PAP correction RemiX IDfiX) was used to measure the chemical composition of individual grains and matrix spots. The amorphous grain ration was assessed by OMPL and total amorphous content calculated by Rietveld-refinement from XRPD results. Newly-formed crystalline components were identified by OM and XRPD. The chemical element distribution and heterogeneity of different textural components was characterized X-ray mapping (XRM), combined with back-scattered electron (BSE) imaging. XRM was performed especially for Al, Si and Na for 0T, 30T and 60T. The resulting maps were further processed by image analyzer software (ImagePro Plus). Low-intensity values were cut out after smoothing the, resulting in images displaying only elevated concentrations.

RESULTS AND DISCUSSION

OMPL and SEM

OMPL revealed that the raw fly ash is composed mainly of spherical and anhedral glassy fragments, anhedral opaque grains and crystalline fragments. Most of the glassy grains have densely scattered gas inclusions. The ratio of the different phases is estimated as 50 - 60 % glassy spherules and grains, 15 - 20 % crystalline fragments and 30 - 35 % opaque grains. Compared to the untreated raw fly ash, the geopolymer samples show even less crystalline fragments. The material is mainly composed of optically isotropic spherules and grains and opaque anhedral grains as well as a fine-grained matrix.

Texture components of the 0T geopolymer sample (raw fly ash based) in thin section consists primarily of spherical glassy particles. Grain size of the spheres ranges from 0.05 to 2.5 mm, most frequently ~ 0.1 mm. The spheres, varying from colourless to dark grey colour, show the presence of internal holes. For most of the spherical grains the volume of the holes exceeds the volume of solid material (indicating that the spherules are fragments of larger aggregates). Other frequent components are the peachstone-like glassy grains, which have usually black, sometimes dark grey colour.

Very few mineral grains and fragments are also found in the samples. Most of the crystalline material was observed in the spherical grains, composed of columnar and needle-like crystals with low interference colours.

Based on optical properties and the XRPD analysis, these are mullite crystals and probably formed during the coal combustion (1000°C). The grains are cemented usually by adjoining surfaces, rarely by crystalline pore-filling cement. Large interstitial volumes remain unfilled – creating closed porosity, making the sample rather brittle, resulting in very low compressive strength (0.4 N·mm^{-2} in Figure 4b). The crystalline cement has a very low birefringence and shows quadratic desiccation cracks.

In contrary to 0T, samples 10T, 20T, 30T and 60T show completely different microstructure. Samples 10T, 20T and 30T show similar microstructure, fragments and finer particles of the original fly ash are surrounded by the fine-grained matrix. Coarser grains display globular, spherical, elongated or anhedral shapes. Arched fragments are also observed among the grains, indicating the fragmentation of larger spherules. Based on optical properties predominant part of the grains is amorphous. Crystalline phases are small angular quartz grains, dispersed elongated mullite crystals or their small aggregates and zeolitic cement in some pore spaces. Few spherical Fe-oxide grains were also identified by SEM+EDS. The matrix of these samples consists of tiny amorphous grains. Sample 60T shows again a different microstructure. The grain size has significantly decreased compared to the other ground samples. It consists of angular and anhedral fragments in fine-grained matrix, with a median of grain size distribution at 13 μm.

X-ray powder diffraction analysis

XRPD was performed on geopolymer samples and U0 (raw fly ash) also. Amorphous content was determined by the "amorphous hump" method with the broad peak included in the Rietveld-refinement. The method was tested on synthetic mixture with 90 % glass + quartz +

ZnO + calcite and results were found to be +/- 0.5 % accurate. This procedure reduced to half the specimen preparation and measurements time, since no specimen with added internal standard had to be investigated. This is important in the case of fly ash and similar materials, since the raw composition cannot be predicted (e.g. for corundum content), using any internal standard requires that the specimen without added material is investigated first.

All XRPD patterns show elevated background, resulting from fluorescence due to the finely distributed, not crystalline Fe-oxides. The U0 sample pattern shows a hump in the range of 14 - 31° 2θ (peak position 22.95) that indicates the Al–Si ± alkaline cations glassy material of the sample. The geopolymer samples have the same hump (Figure 1a), but shifted with 1.8° 2θ right (range 12 - 36° 2θ, peak position 24.75° 2θ) that shows capture of some large cations (probably Na) in the amorphous Al–Si material. However, to determine the accurate composition and atomic arrangement, more sophisticated techniques are required [22].

The composition of the samples calculated by Rietveld-refinement is summarized in Table 4. The X-ray amorphous material content of U0 is 80 wt. %, while that is 3.5 - 7.5 wt. % higher in treated geopolymer samples. Crystalline phases of the U0 comprise SiO_2 minerals, mainly quartz, as well as Al-silicates like mullite. Very little feldspar was detected, in the otherwise regular fly ash composition [23]. According to chemical and mineralogical analysis, the material results in low Ca geopolymer, being less susceptible for acid attack e.g. [24].

Geopolymer samples have similar crystalline phases as raw fly ash, as newly-formed phases zeolite-A (Figure 1b) (hydrous Na-silicate) and sodalite-type structure (STS, with cation substitution) phases occurs. The most abundant crystalline phase was mullite
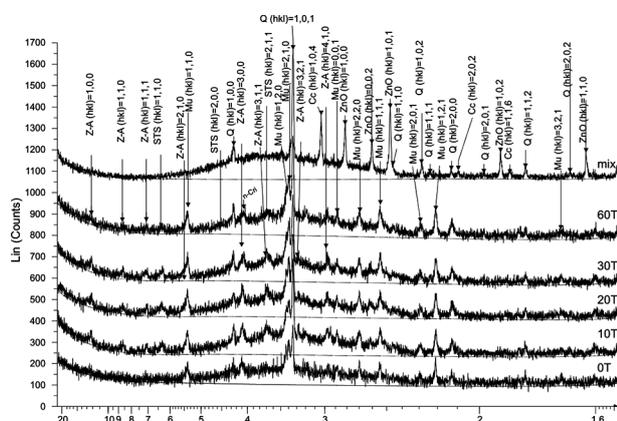

Figure 1a. XRPD graphs of investigated samples. Note the similar position for amorphous hump of glass (mix), geopolymer from unground fly ash (0T) and geopolymer samples (Z-A = zeolitye-A, STS = sodalite type structure, Q = quartz, Mu = mullite, Cc = calcite, ZnO = zincite).
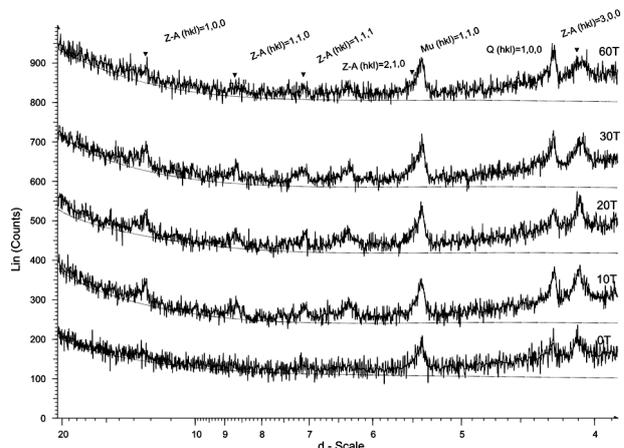
Figure 1b. XRPD graphs of investigated samples, with the peaks of zeolite-A phase magnified, note its absence in the geopolymer from unground and long time ground material (Z-A = zeolitye-A, STS = sodalite type structure, Q = quartz, Mu = mullite, Cc = calcite, ZnO = zincite).

Table 4. Summary of the mineralogical composition of the analysed samples based on Rietveld refinement XRPD analyses.

ICDD no.	Mineral	Formula	Phases					
			0U	0T	10T	20T	30T	60T
046-1045	Quartz	SiO_2	3.48	1.67	2.25	2.27	2.16	2.61
076-0940	Cristobalite high	SiO_2	3.98	0.53	0.57	0.70	0.49	0.40
015-0776	Mullite 2:1	$Al_{4.8}Si_{1.2}O_{9.6}$	12.45	7.78	8.29	8.59	8.77	8.85
089-5894	Maghemite	Fe_2O_3	–	0.13	0.34	0.29	0.00	0.32
083-1658	Albite high	$Na_{0.66}K_{0.33}AlSi_3O_8$	0.09	0.51	0.00	0.00	0.00	0.93
038-0241	zeolite-A	$NaSiAlO_4·2.25(H_2O)$	–	1.20	2.77	2.78	3.18	1.66
052-0145	Sodalite-type structure (STS)	$Na_4Al_3Si_3O_{12}Cl$	–	0.15	0.53	0.59	0.50	0.30
038-0471	Sillimanite	Al_2SiO_4O	–	0.54	0.65	1.26	1.40	1.23
	amorphous (glass)	$Si>Al>Na ± H_2O$	80.00	87.50	84.60	83.50	83.50	83.70

(observed by OMPL also). Another detected Al-silicate was sillimanite (low abundance, not identified OMPL).

The identified mineral phases can be sorted in two groups: 1.) inherited minerals of the raw fly ash: quartz, cristobalite, mullite, feldspar. This composition indicates that Fe, Mg and partly Ca, shown by bulk chemical analysis, are in the amorphous phase; 2.) newly-formed phases that develop by dissolution and recrystallization of the protolith minerals and glass, by NaOH and heat treatment: zeolite-A, sodalite-type structure (STS). The hydration of glass with elevated Na-content (shift of the diffuse peak) resulted in zeolite-A (LTA structure type) and phases of sodalite-type structure, with various cation and anion replacements. Nanocrystalline zeolites are also supposed to be present, associated with the amorphous peak centered at ~ 27 - 29° (2θ) with Cu-K$_α$ (reported in geopolymer samples by [25]). Sillimanite, plagioclase and maghemite were detected in traces.

Comparing the crystalline components for different geopolymer samples, the following characteristics can be drawn. Zeolite-A appears in geopolymer samples, its amount increases gradually from 0T sample till 30T and then decreases for 60T sample; The same trend holds for sodalite-type structure phases, however its amount is much lower than for zeolite-A. The amount of protolith minerals drops significantly in the geopolymer samples. The biggest change is found for mullite and cristobalite, while it is moderate for quartz. The largest drop of mullite and quartz is found for the 0T sample and there is no significant difference for these phases in samples 10T-60T. On contrary, the amount of the amorphous phase increases by 3 - 7 wt. % in the geopolymer samples compared to the raw fly ash one.

Feldspar was detected for 0T and 60T samples with less than 1 wt. % amount. There is no conclusive result to indicate the formation of this mineral during geopolymerization. Thus, it could be considered either a neoformation phase or perhaps an accidental appearance of fragments in this sample only. Crystalline Fe-oxide appears only in small quantities. However, the Fe_2O_3 content of the fly ash was determined for 7.4 - 12.5 wt. %. Since Fe-bearing minerals are absent from samples, Fe most probably is present as dispersed amorphous or nanocrystalline Fe/Fe-oxide. Some Fe-rich spherules were found by SEM, containing Fe_2O_3.

The changes in mineralogical composition revealed by XRPD indicate that the protolith minerals – mullite, cristobalite and quartz – dissolve during the NaOH treatment and solidify partly into Na-Al-silicates (zeolite A and STS) and amorphous Na-Al-Si glass.

EDS and XRM

XRM was performed for all samples and EDS analyses were done in samples: 0T (21 points), 30T (22 points) and 60T (12 points). Points for EDS were selected representative for all textural components: spherical and anhedral grains, central part and outer zone of grains as well as points from the fine grained matrix.

The chemical composition of analysed points show eight major elements: Na, Mg, Al, Si, Ca, K, Fe and O. Traces of Ti occurred in some points, but even in Fe-oxide spherules it was < 1 At. %. All other points show the existence of an Al-silicate material, where the most abundant minor element is Na (most frequently 3 - 4 At. %, but in some grains and in the matrix up to 7.75 At. %). The other four minor elements (Mg, Ca, K, Fe) were usually found < 1 At. %, however in few points their concentration rose up to 2 At. %. The second most abundant minor element was K, in 13 points the concentration rose over 1 At. %. A few outlier points were detected with Mg, Ca or Fe > 4 At. %. No significant difference was recognized between the composition of the three analysed samples (0T, 30T, 60T).

The EDS measurements were found to represent the composition of several phases, since the grain (or crystallite) size of observed minerals is lower than the excitation volume. According to this, the chemical compositions obtained on crystalline parts of samples were applied for normative recalculations. The three main crystalline phases from XRPD (mullite 2:1, zeolite-A and quartz) were used as normative phases. For zeolite-A the nepheline chemical formula was applied, since H_2O content was not determined by EDS (meaning that nepheline composition from EDS refers to zeolite-A). For the normative calculation all Na_2O was considered

as part of nepheline, remaining Al_2O_3 as mullite and the leftover SiO_2 as quartz. The minor components (MgO, CaO, K_2O, FeO) were added to SiO_2 (Figure 2a). For reference, the principal crystalline phase compositions (mullite + sillimanite; zeolite A + sodalite; quartz + cristobalite) from XRPD are shown (squares in the triangle diagram). The diagram shows that the measured points are enriched in SiO_2 relative to the XRPD results, indicating the amorphous + crystalline material in the excitation volume.

Distribution of Si versus Al in the matrix is shown in Figure 2b for the analysed points. Only the outlier points with elevated Fe-content were excluded. Plotted data is recalculated to a chemical formula with 13 O atoms. For comparison, the theoretical chemical composition of the crystalline phases by XRPD are also plotted in the graph. The composition of measured points – taken primarily from amorphous Al-silicate phases – lies along the line between pure SiO_2 and the Al-silicate phases (sillimanite, mullite), identified by XRPD. The composition of zeolite-A, as the main newly-formed crystalline phase, fits also well to the distribution. Most of the measured points lie left from the zeolite-A composition and far left from the Al-silicate phases towards the SiO_2. This trend is showing that the amorphous Al-silicate material is enriched in SiO_2 relative to the Al-silicate phases indicated by XRPD.

For sample 30T, there is a wider scatter range of Na-content. There are also points with Na-depleted or enriched compositions, like in 0T and 60T, but for 30T some Na-dominant compositions were also found. These points were measured in highly porous anhedral grains or in the intergranular matrix.

The amount of newly-formed hydrated phases observed by EDS is the lowest in 0T and 60T samples. This correlates with the XRPD results (squares in the triangle diagram), where less zeolite-A and STS was detected from the 0T and 60T samples than from 10T, 20T and 30T.

Generally elevated Na-content was detected in the interstitial fine-grained matrix, especially for the 30T sample. Si and Al are abundant mainly in anhedral and spherical grains and in rarely occurring grains with crystal shape. No such regularity was found for, Mg, Ca, Fe or K. They appear more evenly distributed, concentrated in several grains or small spherules.

The BSE image (Figure 3a, BSE) shows the wide chemical inhomogeneity of the fly ash material. The Na-Kα map (Figure 3a, Na-Kα image) shows high concentration in the matrix (dots 14 and 19), and especially at junction points of the grains. Elevated concentration is found also within some anhedral grains (dots 13, 16 and 18) that have a microporous texture on the BSE image. These grains show also high concentration of Al with lower Si, and they correspond to glass spherules. The Al- and Si-content (Figure 3a, Al-Kα image) is more elevated in fly-ash fragments and not in the matrix. Dots 1, 2, 6, 11 and 12 represent mullite or similar compositions, these were found nanocrystalline according to OM. The NaOH activation and binding effect on fly ash grains is visible on the border of grain measured in dots 1, 2, 3, 3a and 4. While the core of the grain is Si-rich, an Al-Na silicate formation is observed with Na-enrichment outwards from its core. In contrary, XRM of 60T shows finer grain sizes, as a result of grinding (Figure 3b, BSE). Accordingly, the NaOH solution penetrated the matrix more efectively, thus we have more abundant and evenly distributed Na-content (Figure 3b, Na-Kα image). Enhanced Na-content appears at grain boundaries and in the interstitial matrix, while high Al-content is characteristic for anhedral grains (Figure 3b, Al-Kα image). The Si-rich grains are also broken up and a more

Figure 2a. Composition of EDS measurement points (dots) recalculated to three normative components: nepheline (dehydrated zeoliteA), mullite 2:1, quartz. Squares: reference bulk composition calculated based on crystalline phases from quantitative XRPD.
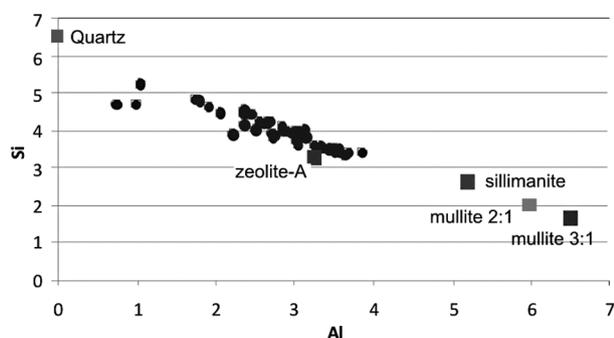

Figure 2b. Distribution of Si as a function of Al (dots) from chemical composition of EDS measurement points from samples 0T, 30T, 60T. All chemical compositions were recalculated for 13 oxygens. Squares: reference bulk composition of mineral phases identified by XRDP.
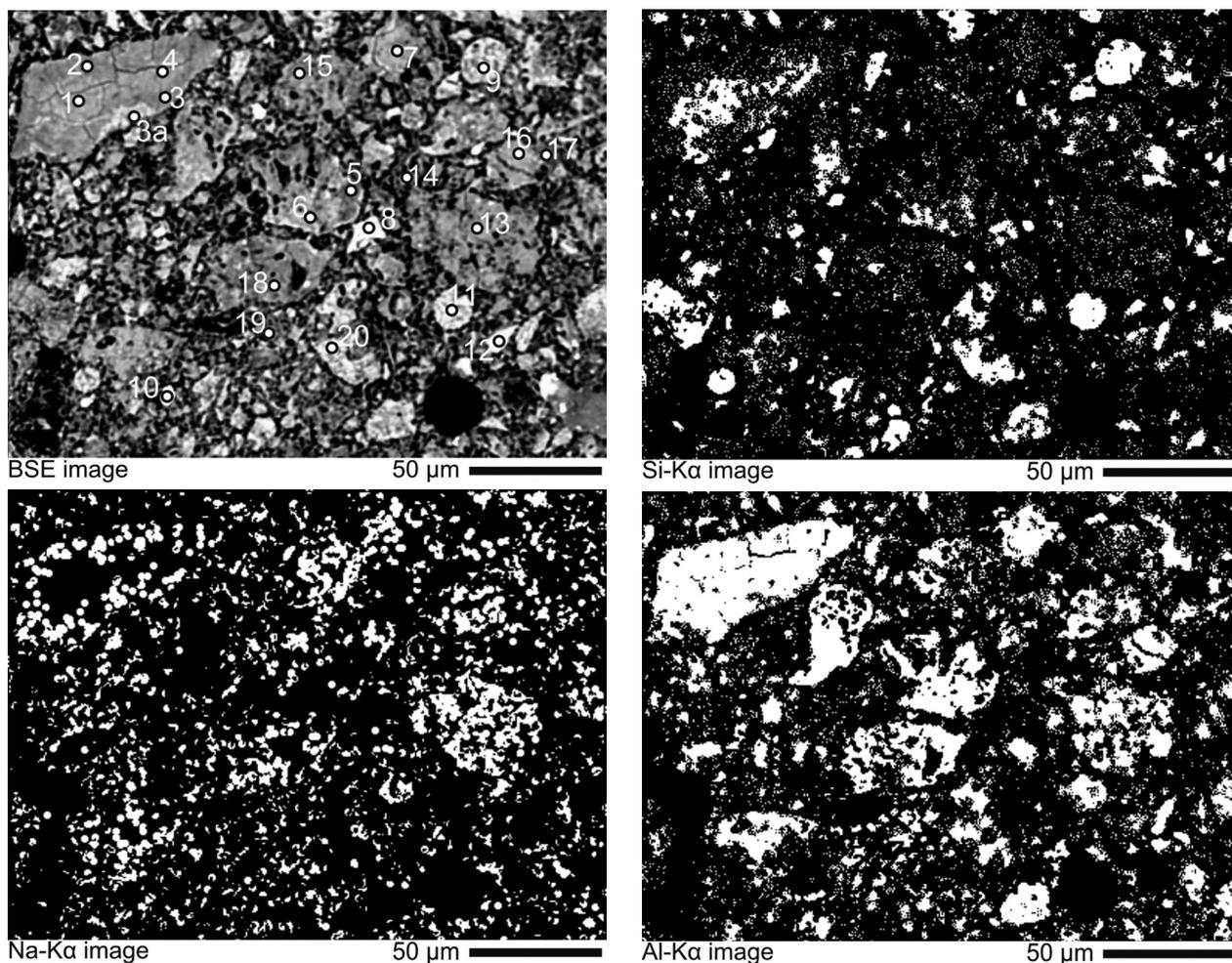
Figure 3a. BSE images with the measurement points and XRM images for sample 0T.

homogeneous distribution was obtained (Figure 3b, Si-Kα image).

Material balance calculation was completed for dissolved and precipitated components based on XRPD results and crystalline phase compositions. It shows that for each treated sample about 3.5 % (total mass) SiO_2 is dissolved from cristobalite, 0.8 - 1 % SiO_2 from mullite and other 0.9 - 1.8 % from quartz. Some 2.8 - 3.6 % Al_2O_3 is dissolved from mullite. The newly-formed phases take about 0.5 % SiO_2 for samples T0 and T60 and about 1.2 % SiO_2 for T10, T20, T30 samples, while 0.4 - 0.6 % Al_2O_3 for samples T0 and T60 and about 1.1 % Al_2O_3 for T10, T20, T30 samples. The rest of SiO_2 and Al_2O_3 is added to the amorphous phase.

Particle size distribution and uniaxial compressive strength

The reactivity of fly ash can be improved significantly by mechanical activation [26]. Based on this fact a comparative systematic investigation was fulfilled on the geopolymerisation process when the grinding time was the variable parameter. For the mechanically activated fly ash samples (10T, 20T, 30T, 60T) produced by grinding, size distribution was measured. Median of the particle size distribution is 39 μm for 10T, 24 μm for 20T, 17 μm for 30T sample and 13 um for 60T sample (Figure 4a).

The specific surface area (SSA) determined by BET method and calculated from the particle size distribution data of the raw and ground fly ash is show in Table 5. The BET value, representing the total surface of the particles including micro and mezo-pores, increases gradually as function of grinding time from initial value of 4.655 $m^2 \cdot g^{-1}$ up to 8.428.8 $m^2 \cdot g^{-1}$ after 60 min grinding time. Same SSA increase trend was observed regarding the "outer" SSA values which increased from 501 $cm^2 \cdot g^{-1}$ to 3293.5 $cm^2 \cdot g^{-1}$ after 60 min milling. The significant difference between the values of the various specific surface area types can be explained by the porous structure of the fly ash particles.

After 7 days of ageing, the compressive strength of the geopolymer specimens was determined. The effect of mechanical activation on the specific surface area of fly ash and compressive strength of specimens can be observed in Figure 4b. The weakest geopolymer resulted from raw fly ash (0T) which has only 0.40 MPa
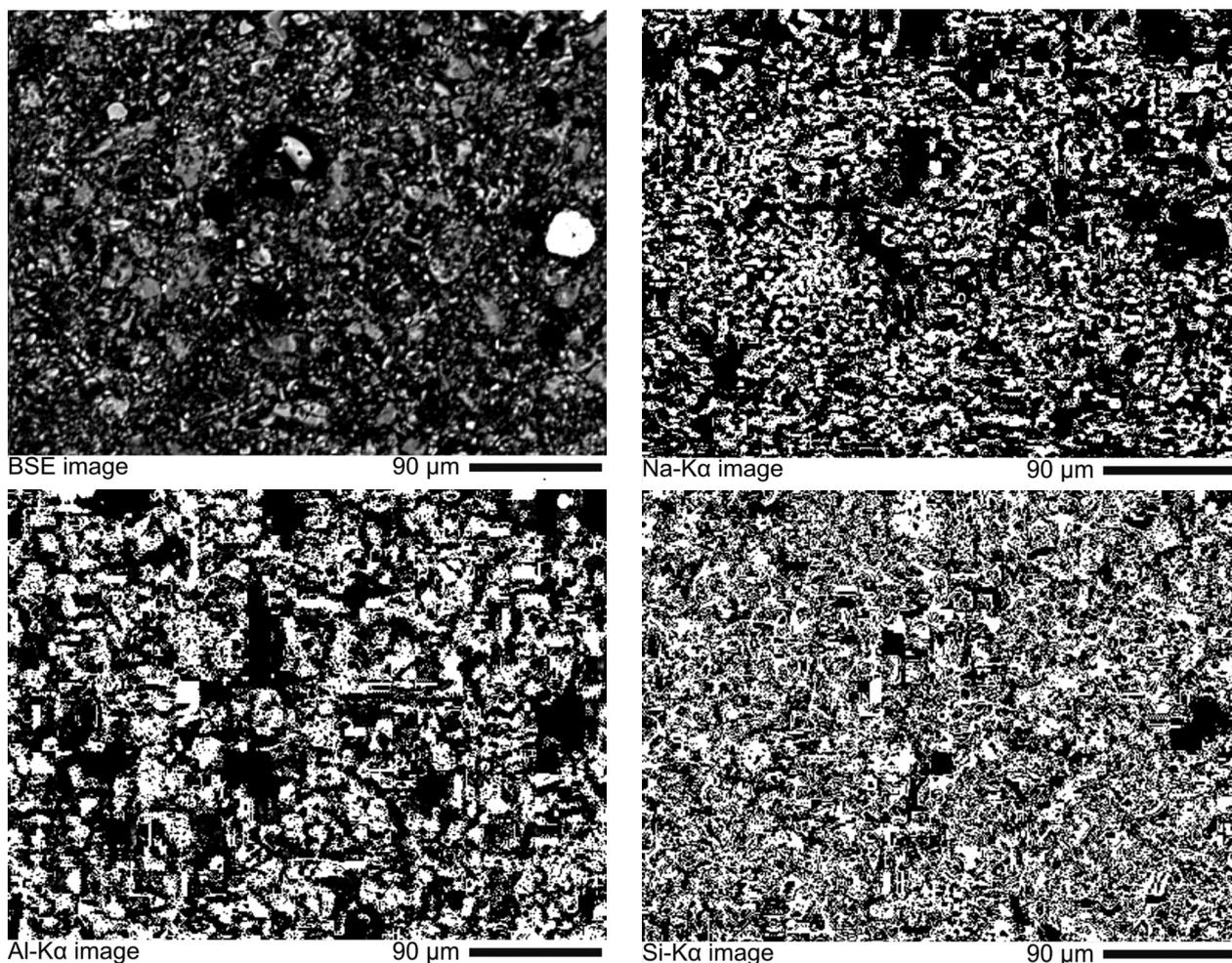
Figure 3b. BSE images with the measurement points and XRM images for sample 60T.

of compressive strength. With longer milling time the strength increased significantly until reached the maximum value for 30T (SSA = 2500 cm²·g⁻¹, 10.66 MPa), than slightly decreased in sample 60T, in spite of increasing specific surface area. The first reason of the change in compressive strength increase is the aggregation [27] of the lowest sized fly ash (secondary) particles. According to these results, the highest compressive strength can be achieved with a milling time of 30 min and a specific surface area of ~ 2500 cm²·g⁻¹.

From Figure 4b it can be stated that the relation between compressive strength and fly ash fineness is not directly proportional. Similar behaviour was found by

Table 5. Specific surface area of the raw and ground fly ash samples.

	BET surface area (m²·g⁻¹)	"Outer" surface area (cm²·g⁻¹)
Raw fly ash	4.655	501.37
Ground for 10 min	5.472	1513.97
Ground for 20 min	6.805	1960.63
Ground for 30 min	7.649	2469.94
Ground for 60 min	8.428	3293.51

Kumar et al. (2007) observing, that higher specific surface area does not result obviously in higher mechanical stability of the geopolymer. Corelation between strength increase, and zeolite-A and sodalite formation (XRPD) was found.

CONCLUSIONS

The present paper summarizes the analytical results on geopolymer research dealing with geopolymer production using ground fly ash. Based on the laboratory experimental results the following conclusions can be drawn. The tested deposited Class F fly ash treated with caustic process liquor originated from Ajka Alumina Plant (Hungary) is suitable for geopolymer production

The reactions that result in geopolymer hardening were found to produce crystalline components like zeolite-A and sodalite structure materials; zeolite-A as a newly formed crystalline species is described rarely in literature. The amorphous content quantification was proved to be useful and accurate, results being reinforced by chemical investigations and experiment with synthetic mixture also; this procedure may cut substantial costs of geolpolymer materials investigations, by the elimination of the added internal standard method. Na diffusion into
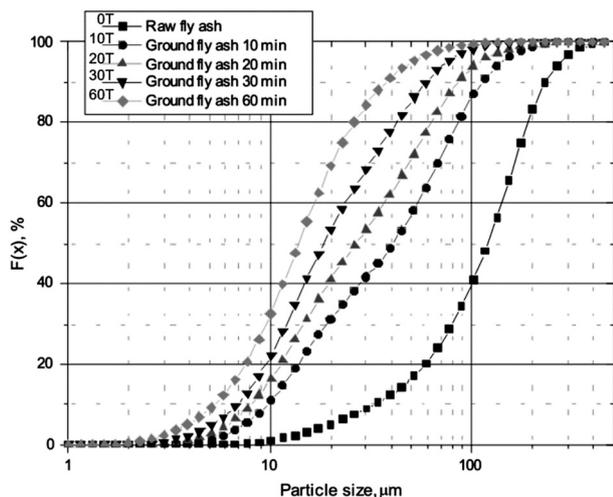
Figure 4a. Grain size distribution of ground fly ash material, before alkali-activation. Note the shift of distribution towards lower sizes, within the same range.

Figure 4b. Compressive strength of geopolymer as function of specific surface area of fly ash.

the amorphous phase was detected by the shift of the "amorphous hump" towards lower d(Å)-values.

By redistributing chemical components on the crystalline components according to quantitative XRPD, we successfully gained approximation on the amorphous materials chemical composition. XRPD analysis of crystalline phases indicates intensive dissolution of the original ground fly ash components (Al-silicates and SiO_2) and formation of Na-Al-silicate phases by activity.

Appropriate texture should be produced for optimal geopolymer production, taking into consideration the particle size distribution, internal structure and shape of the remaining particles. According to our results, this is found in the case of 30T sample, but further detailed experiments should be carried out in the grinding time range of 30 to 60 minutes.

Intensive Na diffusion and replacement was detected for ground samples. By XRM it was found that Na diffusion and replacement takes place not only in the fine-grained matrix but also in the porous, cavernous glassy grains. In the most long time ground 60T sample more overlapping between Si and Na is observed, although zeolite-A formation is prohibited. The appearance of albite in this material may lead to a new alkali-activation reaction, although further experiments are needed to map out this pathway.

The mechanical activation of the raw fly ash has a positive effect on the geopolymerisation, the fly ash fineness – compressive strength relation curve has maximum point at 2500 $cm^2 \cdot g^{-1}$ SSA (10.66 MPa), so the optimal grinding time was 30 min; grinding rises the number of free Al and Si sites on glass nanograins, thus increasing the seeding of crystallites. The mechanical strength of geopolymer became 26.7 times higher using the ground fly ash as a geopolymer component in comparison with raw (unground) fly ash.

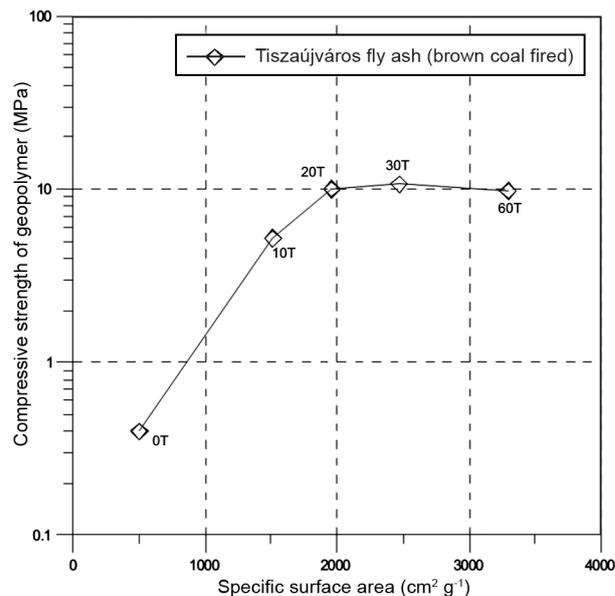The result of overmilling is that geopolymerisation is reduced to the interstitial matrix in sample 60T. Reduced porosity restricts the element mobility necessary for diffusion and replacement within grains. Overmilling results also in agglomerating, thus only the most compacted parts of the vitreous granular material remain as grains, reactivity of the grains being reduced compared to less ground (10T, 20T, 30T) samples.

REFERENCES

1. Temuujin J., Williams R. P., van Riessen A.: Journal of Material Processing Technology *209*, 5276 (2009).
2. Xu H., van Deventer J.S.J.: International Journal of Mineral Processing *59*, 247 (2000).
3. Palomo, A., Grutzeck M. W., Blanco, M.T.: Cement and Concrete Research *29*, 1323 (1999).
4. Davidovits, J.: *Geopolymer Chemistry and Applications*, 3rd edition, Insitute Géopymére, Saint-Qeuntin, 2011.
5. Davidovits J.: J. Therm. Anal. *37*, 1633 (1991).
6. Perera, D.S., Uchida,O., Vance,E.R. & Finnie,K.S.: J. Mater. Sci. *42*, 3099 (2007).
7. Mitash S. N.: ENVIS Newsletter. Vol.2 No. 6. (2007).

(available online http://parisaramahiti.kar.nic.in/11.Fly%20 ash%202007-01.pdf, accessed 04.11.2014.)

8. Feuerborn H. J.: World Coal Ash Conference, May 9-11, 2011, Denver USA. (available on-line, http://www.flyash. info/2011/007-feuerborn-2011.pdf accessed 04.11.2014.)

9. Cao D.-Z., Selic E., Herbell J. D.: Journal of Zheijang University Scientific Acta *9*, 681 (2008).

10. Kumar, R. Kumar, T.C., Bandopadhyay A., Mehrotra S.P.: Advances in Applied Ceramics *106*, 120 2007.

11. van Deventer J.S.J., Provis J.L., Duxson P., Lukey G.C.: Journal of Hazardous Materials A *139,* 506 (2007).

12. Kumar S., Kumar R.: Ceramics International *37*, 533 (2011).

13. Temuujin J., Okada K., Jadambaa T. S., MacKenzie K. J .D., Amarsanaa J.: J. Eur. Ceram. Soc. *23*, 1277 (2003).

14. Hounsi A. D., Lecomte-Nana G. L., Djétéli G., Blanchart P.: Construction and Building Materials *42*, 105 (2013).

15. Mucsi G., Csőke B., Molnár Z. in: Proceedings of the 12th International Mineral Processing Symposium, p. 1235-1242, 6-8 October 2010, Cappadocia Nevsehir, Turkey. ISBN: 978-975-491-295-1,.

16. Somna K., Jaturapitakkul C., Kajitvichyanukul P., Chinda-prasirt P.: Fuel *90*, 2118 (2011).

17. Diaz E.I., Allouche E.N., Eklund S.: Fuel *89*, 992 (2010).

18. van Riessen A., Chen-Tan N.: Fuel *106*, 569 (2013).

19. Paul K. T., Satpathy S. K., Manna I., Chakraborty K. K., Nando G. B.: Nanoscale Res. Lett. *2*, 397 (2007).

20. Fu X., Li Q., Zhai J., Sheng G., Li F.: Cement & Concrete Composites *30*, 220 (2008).

21. van Jaarsveld J.G.S., van Deventer J.S.J., Lukey G.C.: Materials Letters *57*, 1272 (2003).

22. White C. E.: Zeitschrift für Kristallographie - Crystalline Materials, Analysis of Complex Materials *227*, 304 (2012).

23. Thokchom S., Ghosh P., Ghosh S.: International Journal of Recent Trends in Engineering, *1*, 36 (2009a).

24. Thokchom S., Ghosh P., Ghosh S.: International Journal of Chemical and Biological Engineering 2, 20 (2009b).

25. Provis J. L., Lukey G. C., van Deventer J. S. J.: Chem. Mater. 17, 3075 (2005).

26. Csőke, B., Mucsi, G., Opoczky, L., Gável, V.: Cement International 6, 86 (2007).

27. Juhász, A. Z.-Opoczky, L.: *Mechanical activation of minerals by grinding: pulverizing and morphology of particles*, Akadémiai Kiadó Budapest, 1990.